

Article

Electrophoretic Deposition of Graphene Oxide and Reduced Graphene Oxide on the Rutile Phase of TiO₂ Nanowires for Rapid Reduction of Cr (VI) under Simulated Sunlight Irradiation

Subagja Toto Rahmat ¹, Nurhaswani Alias ¹, Rajesh Kumar ², Wai Kian Tan ^{3,*}, Go Kawamura ⁴, Atsunori Matsuda ⁴ and Zainovia Lockman ^{1,*}

¹ Green Electronic Nano Materials Group, Nanomaterials Niche Area, Engineering Campus, School of Materials and Mineral Resources Engineering, Universiti Sains Malaysia, Nibong Tebal 14300, Malaysia

² Department of Mechanical Engineering, Indian Institute of Technology Kanpur, Kanpur 208016, India

³ Institute of Liberal Arts & Sciences, Toyohashi University of Technology, Toyohashi 441-8580, Aichi, Japan

⁴ Department of Electrical and Electronic Information Engineering, Toyohashi University of Technology, Toyohashi 441-8580, Aichi, Japan

* Correspondence: tan@las.tut.ac.jp (W.K.T.); zainovia@usm.my (Z.L.)

Abstract: Hexavalent chromium is very carcinogenic, and it is, therefore, important to remove it from wastewater prior to disposal. This study reports the photoreduction of Cr(VI) under simulated sunlight using graphene-derived TiO₂ nanowire (TNW) composites. Electrophoretic deposition (EPD) of graphene oxide (GO) and reduced graphene oxide (rGO) was carried out on rutile phase TNWs. The TNWs were fabricated by thermal oxidation of titanium foil in the presence of 1M potassium hydroxide mist at 750 °C. The TNWs uniformly covered the surface of the titanium foil. EPD of GO or rGO was done as a function of time to produce deposits of different thicknesses. The photocatalytic performances of the GO/TNWs or rGO/TNWs were tested to reduce Cr(VI) under visible light. The performance of rGO/TNWs in reducing Cr(VI) was better than GO/TNWs. A 10-second-deposited rGO on TNW samples can reduce 10 mg/L Cr(VI) within 30 min under visible light, likely as a result of the high electron transfer from rGO to TNWs accelerating the Cr(VI) reduction.

Keywords: graphene oxide; reduced graphene oxide nanosheets; titanium oxide nanowires; electrophoretic deposition; photocatalysis; hexavalent chromium reduction



Citation: Rahmat, S.T.; Alias, N.; Kumar, R.; Tan, W.K.; Kawamura, G.; Matsuda, A.; Lockman, Z. Electrophoretic Deposition of Graphene Oxide and Reduced Graphene Oxide on the Rutile Phase of TiO₂ Nanowires for Rapid Reduction of Cr (VI) under Simulated Sunlight Irradiation. *Catalysts* **2022**, *12*, 1282. <https://doi.org/10.3390/catal12101282>

Academic Editor: Kwun Nam Hui

Received: 6 September 2022

Accepted: 17 October 2022

Published: 20 October 2022

Publisher's Note: MDPI stays neutral with regard to jurisdictional claims in published maps and institutional affiliations.



Copyright: © 2022 by the authors. Licensee MDPI, Basel, Switzerland. This article is an open access article distributed under the terms and conditions of the Creative Commons Attribution (CC BY) license (<https://creativecommons.org/licenses/by/4.0/>).

1. Introduction

Chromates are used in many industrial processes, including metal fabrication, leather tanning, pulp and paper production, and electroplating [1]. Chromic acid, for example, has been used for electroplating chromium onto metal components to improve their corrosion resistance and increase their abrasive wear. In a typical electroplating process, a metal to be plated is immersed in a sodium cyanide or caustic soda solution as a pretreatment, followed by cleaning and rinsing before being transferred to a chrome bath for chromium plating. After this process, the metal parts are rinsed again. All of these processes result in a large volume of wastewater containing released cyanide and acidic Cr(VI). Cr(VI) is carcinogenic, highly corrosive, and very toxic [2,3]—considerably more toxic than Cr(III)—and hence must be removed from the wastewater. Chemical reduction of Cr(VI) to Cr(III) is commonly carried out to remove Cr(VI) from wastewater, for example, by using sulfur dioxide gas or sodium bisulfite and sulfuric acid. That treatment lowers the Cr(VI) concentration from the effluent, but not to zero, and it generally involves subsequent adjustment of the solution to precipitate the Cr(III) ions. Chemical reduction utilizes hazardous chemicals and can generate dangerous by-products and, potentially, the evolution of toxic gases.

Therefore, an alternative process that results in zero Cr(VI) effluent without the use or release of toxic chemicals or gases is sought. Among the strategies for total Cr(VI) removal using a more benign process, photocatalytic reduction is considered a promising approach [3]. In photocatalytic reduction, the Cr(VI) reduction occurs with free electrons that are generated when a semiconductor photocatalyst is illuminated with light with an appropriate amount of energy [4]. Titanium dioxide (TiO₂) is a well-known and efficient semiconductor photocatalyst that is also non-toxic, biologically and chemically inert, stable, and inexpensive [5].

TiO₂ can be synthesized in the form of one-dimensional (1D) nanostructures, which is beneficial because 1D nanomaterials have a large surface-to-volume ratio. This translates to a high-reactivity catalyst, thus leading to an enhanced photocatalytic performance [6]. There are many ways to synthesize 1-D TiO₂ nanostructures containing different morphologies, such as nanotubes, nanowires, and nanorods [7–11].

In this work, thermal oxidation of titanium was conducted in the presence of 1M potassium hydroxide (KOH) mist to produce rutile TiO₂ nanowires (TNWs). Oxidation is a simple process that can produce highly crystalline TNWs in a short processing time. Nevertheless, rutile TiO₂ is a wide-band-gap semiconductor (3.2 eV) and, hence, can only produce free electrons under ultraviolet (UV) light illumination (wavelength range <400 nm) [12,13]. Rutile TiO₂ is thus not very photoactive under sunlight. In efforts to produce a semiconductor photocatalyst that can be activated under sunlight, TiO₂ is often doped or coupled with organic materials such as graphene. The coupling has been shown to increase the visible light activity of TiO₂ by creating a new energy level within the energy band gap [14–16]. However, the defect levels can also act as recombination centers for the photogenerated electron-hole pairs [17]. In addition, graphene, which is known for various applications, such as electromagnetic interference shielding [18], supercapacitors [19–21], and other energy storage applications [22,23], when coupled with TiO₂, does not create defect states although electron transfer is expected [24]. This will create more electrons in the semiconductor. As a semi-metal with a very small band gap, graphene can also extend light absorption of TiO₂ to the visible light spectrum [25,26], and, hence, sunlight activation can be achieved.

Methods to combine TiO₂ with graphene or reduced graphene oxide (rGO) may vary depending on the thickness of the layers desired, the way the rGO is produced, and the features and geometry of the substrate. In this work, graphene oxide (GO) was used in an electrophoretic deposition (EPD) method to fabricate GO/TNWs. Another set of experiments was carried out by reducing GO to form reduced GO (rGO), and EPD was used to produce rGO/TNWs. EPD is a well-known technique whereby suspended particles are impelled from the suspension medium to a substrate using an electric field, and it has been shown to be a successful method for GO and rGO deposition [27]. Herein, GO and rGO in liquid suspension were used with deposition done on titanium foil comprising the TNWs. Nanocatalysts in dispersed particles have been reported to possess good catalytic performance due to a large, accessible surface area for a reaction to occur. However, they tend to form superfine particles in water, making it difficult to separate them from the treated water; thus, they become secondary pollutants in the water system.

A supported photocatalyst is proposed to address this problem: rGO/TiO₂ has several significant advantages, including good photoelectron injection from one material to another and simple post-separation and recycling of the system from the effluent after treatment. Moreover, to date, little work has explored the effect of EPD time and, therefore, the effect of the thickness of the GO or rGO on the photocatalytic reduction of Cr(VI) to Cr(III). It is anticipated that a thicker deposit will mean more electron transfer can occur, which may improve the reduction process of Cr(VI). In addition, the study on Cr(VI) reduction using supported rGO/TNWs is also rather limited.

2. Results and Discussion

Figure 1 shows a typical low-magnification FESEM image of the TNWs synthesized at 750 °C. As can be seen, the pristine sample comprises TNWs that uniformly cover the titanium foil. The length of the TNWs is ca. 500 nm, and the diameter ranges from 10 to 50 nm. The growth mechanism of the TNWs may be due to preferential oxide growth in the presence of the KOH mist. Accumulating a K-rich compound, such as $K_2Ti_6O_{13}$, at the sides of the growing TNWs, impedes radial growth and allows for c-axis growth [6].

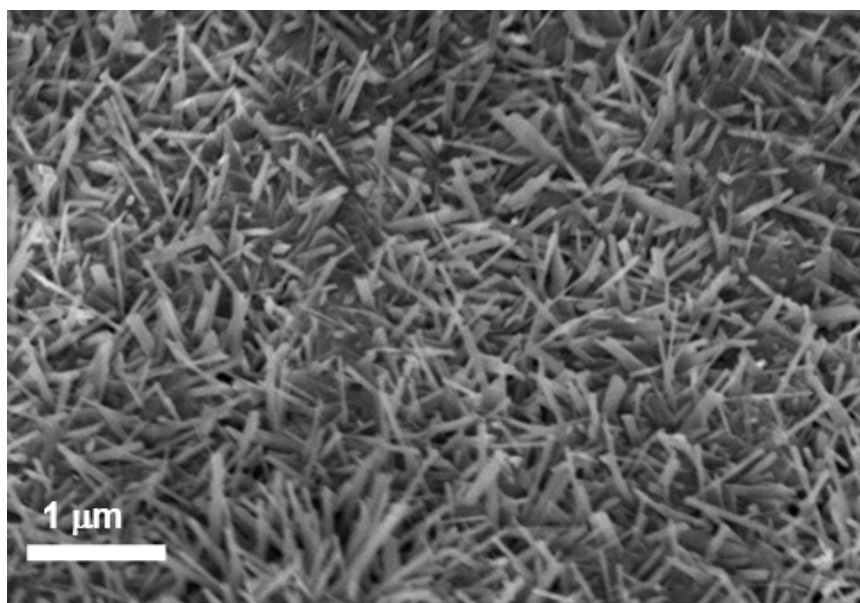


Figure 1. Surface morphology of pristine TNWs before GO/rGO nanosheet deposition.

Surface FESEM morphologies of GO and rGO deposited on the TNWs using EPD at several deposition times are shown in Figures 2 and 3, respectively. Images on the left are low-magnification (100 μm), whereas higher magnification (1 μm) surface morphologies can be seen in the right column. From the low-magnification images, it can be observed that the amount of GO nanosheets and rGO nanosheets deposited on the surface of the TNWs increased as EPD time increased, as shown in Figures 2 and 3a–d-i. Higher magnification images, in Figures 2 and 3a–d-ii, were taken at the edge of the GO and rGO. In these images, the clear presence of TNWs with GO and rGO can be seen.

The XRD pattern of the TNWs, shown in Figure 4a, exhibited the presence of a rutile phase TiO_2 structure (ICSD No. 98-001-7802), with dominant diffraction peaks present at $2\theta = 27.5^\circ$, 36.1° , and 54.3° . These diffraction peaks correspond to (110), (011), and (121) rutile- TiO_2 , respectively. The appearance of two diffraction peaks at 11.4° and 29.8° can be ascribed to the $K_2Ti_6O_{13}$ phase (ICSD No. 98-001-1919), and the presence of KOH during the oxidation process may have resulted in this phase, which inhibited radial growth and induced the formation of 1D TNW structure. The XRD patterns of the GO/TNW and rGO/TNW samples show a similarity to the TNW sample, which indicates that the presence of GO or rGO does not affect the crystal planes of the underlying TNWs. No typical diffraction peaks of carbon species were observed in either sample, which may be due to the low quantity and relatively low diffraction intensity of GO or rGO [28].

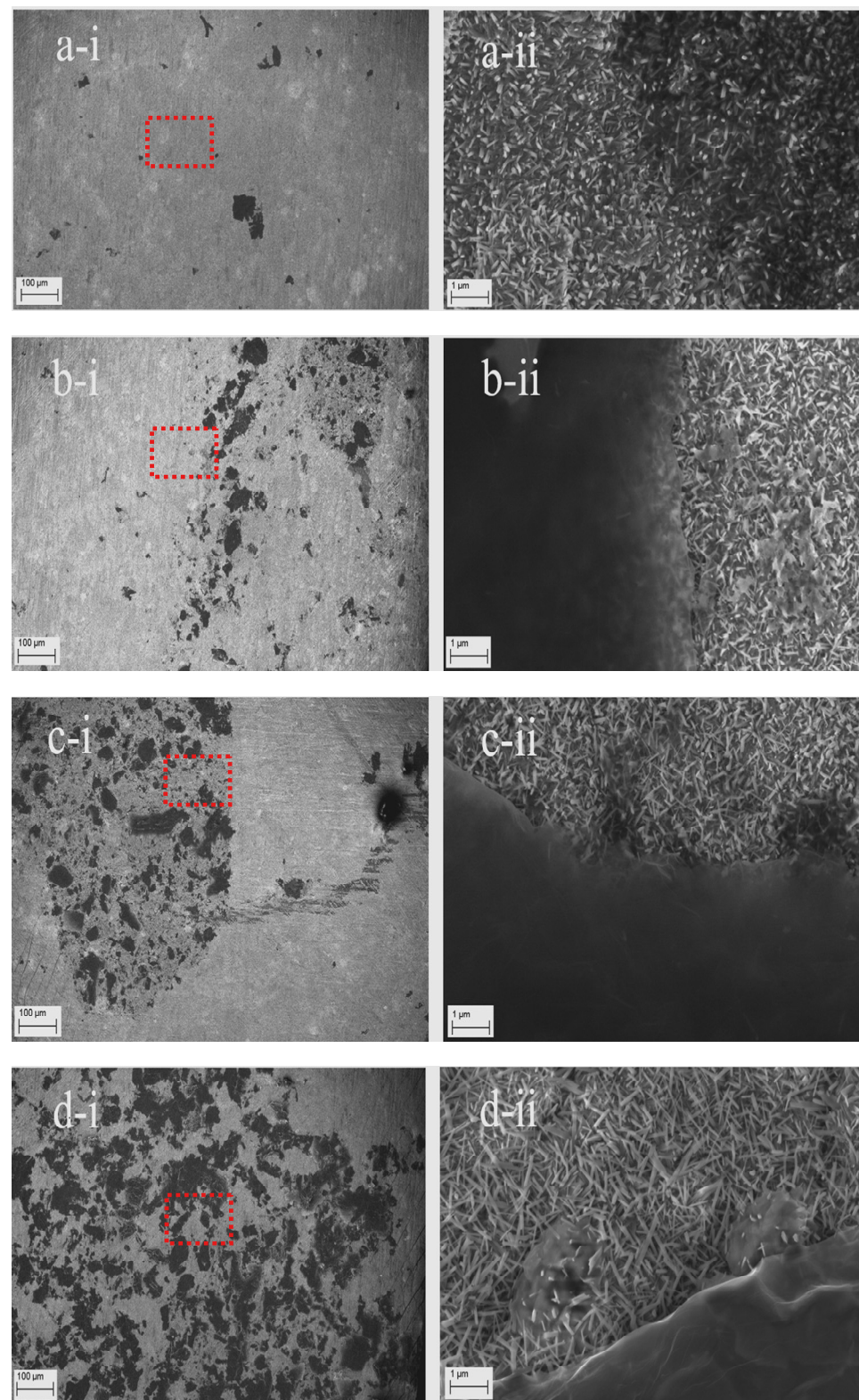


Figure 2. FESEM images of GO deposited on TNWs using EPD with different deposition times: (a) 10 s; (b) 30 s; (c) 1 min; and (d) 5 min. Low-magnification images: left side ((a-i) to (d-i)) and high-magnification images: right side ((a-ii) to (d-ii)).

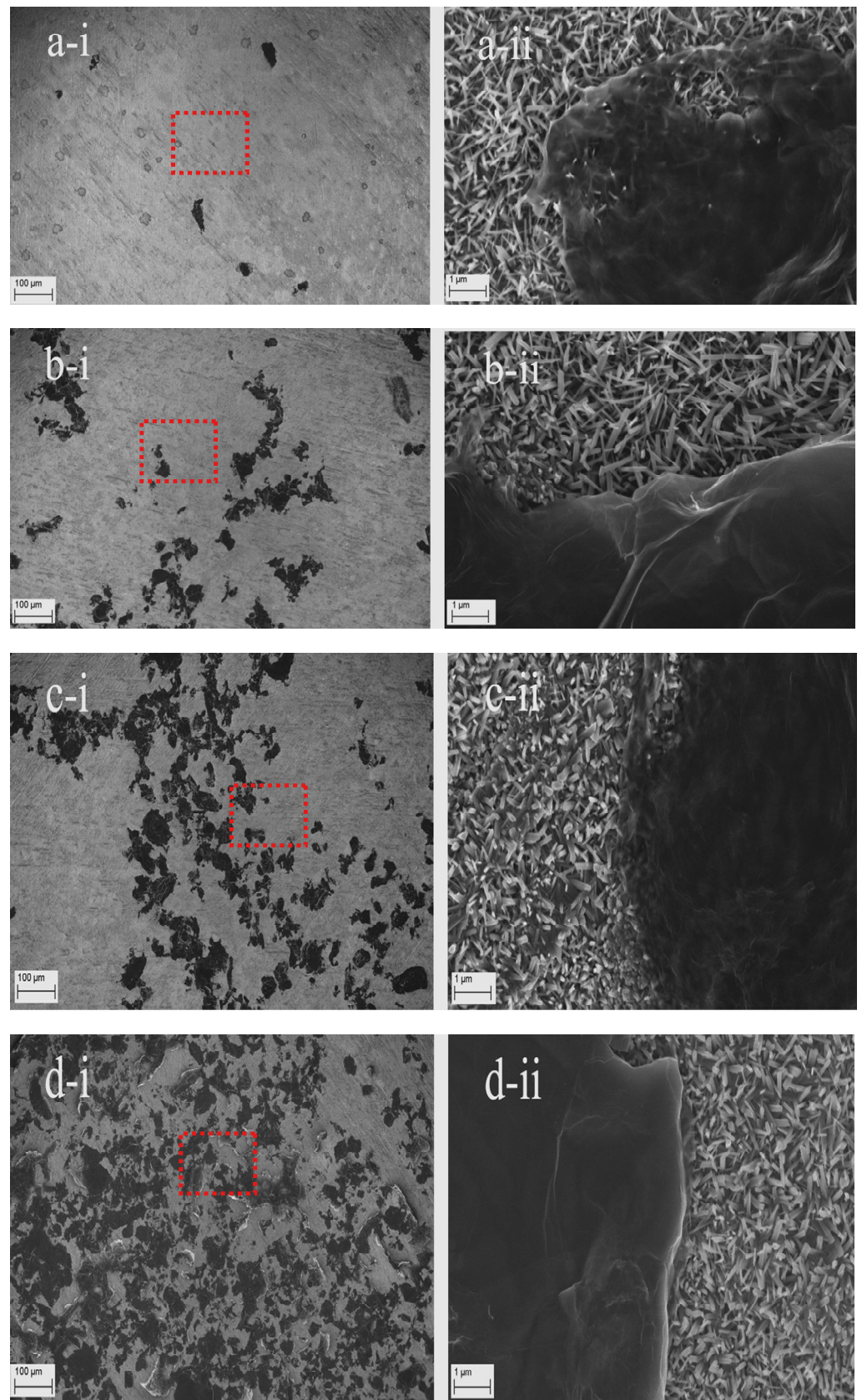


Figure 3. FESEM images of rGO deposited on TNWs using EPD with different deposition times: (a) 10 s; (b) 30 s; (c) 1 min; and (d) 5 min. Low-magnification images: left side ((a-i) to (d-i)) and high-magnification images: right side ((a-ii) to (d-ii)).

Raman spectra (see Figure 4b,c) further indicate the existence of rutile TiO_2 peaks ($B_{1g} = 142 \text{ cm}^{-1}$; $E_g = 449 \text{ cm}^{-1}$; $A_{1g} = 613 \text{ cm}^{-1}$) [29,30], and a $\text{K}_2\text{Ti}_6\text{O}_{13}$ peak (at approximately 240 cm^{-1}) [31] for all samples studied. The broad Raman peaks present at 1358 cm^{-1} and 1605 cm^{-1} correspond to D- and G-bands, respectively, and result from the presence of graphene derivatives as GO/rGO nanosheets in the GO/TNW and rGO/TNW samples but not in the pristine TNW sample. These Raman peaks belong to D-band and G-band carbon atoms from GO or rGO that are on the surface of the samples [19,22,32–35]. The stronger intensity of D over G peaks (I_D/I_G) may indicate a reduction of oxygen-functional groups in GO [36]. All Raman spectra for rGO/TNW samples show a higher intensity of D over G, thus indicating effective reduction from GO to rGO using chemical reduction with ascorbic acid.

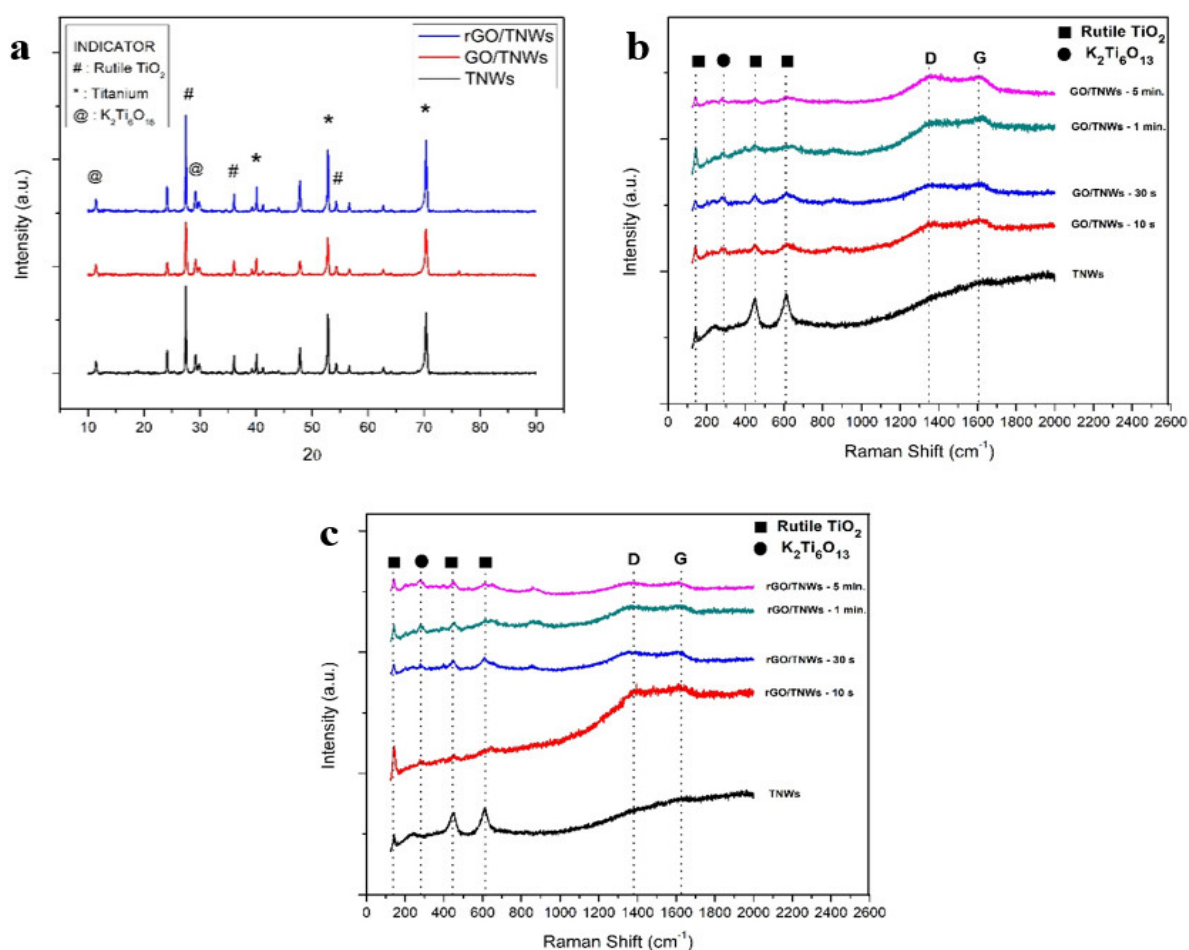


Figure 4. (a) XRD patterns of TNWs, GO/TNWs, and rGO/TNWs samples; (b) Raman spectra of TNWs and GO/TNWs samples with different deposition times; and (c) Raman spectra of TNWs and rGO/TNWs samples with different deposition times.

Possible interactions between GO or rGO with TiO_2 , as well as the chemical state of all the elements, can be studied with a high-resolution XPS. The high-resolution XPS images of C 1s core spectra are shown in Figure 5a for both GO/TNWs and rGO/TNWs. A peak at 285.1 eV, assigned to C-C from the sp^3 hybridized graphitic carbon atoms, can be detected for both samples. Deconvolution of the peak reveals several other peaks, such as for C=C bonds at 284.4 eV or C-C from sp^2 hybridized graphitic carbon atoms [37,38]. Oxygen-bound species can be seen at around 286–287 eV, possibly from C-O, carbonyl or carboxyl C=O, and C-O-C. It can only be detected for the GO/TNWs sample because GO contains more of such oxygen-functionalized species compared with rGO. Chemical reduction using ascorbic acid, therefore, significantly reduces the number of oxygen-bound

species and successfully reduces GO to rGO [37]. The XPS results of O1s core level spectra are displayed in Figure 5b. The XPS peaks at 529.8 eV in rGO/TNWs and 530.6 eV in GO/TNWs correspond to the Ti-O bond of TiO₂ [37,39]. A small peak at ca. 531.8 eV is likely to come from OH absorbed on the surface of the oxide [39]. The oxygen-bound species C-O is detected at 532.7 eV in GO/TNWs but not in rGO/TNWs, further confirming the reduction from GO to rGO.

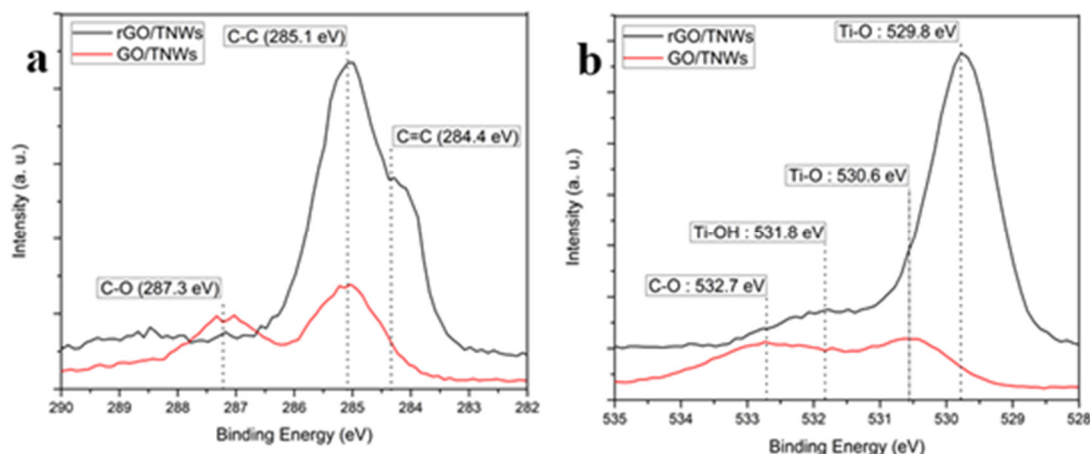


Figure 5. (a) Typical high-resolution XPS spectra of C 1s and (b) O 1s XPS spectra of rGO/TNW and GO/TNW samples.

The photocatalytic performance of TNW, GO/TNW, and rGO/TNW samples in reducing Cr(VI) ions under visible light is illustrated in Figure 6. As can be seen, the reduction on the TNWs was negligible until GO or rGO was deposited onto them. For the GO/TNWs, the reduction performance improved as the deposition of GO was extended. The thicker the GO, the faster the removal of Cr(VI) that was observed. The maximum reduction of Cr(VI) was achieved for GO/TNWs with a 5-min deposition of GO on the TNWs. However, the reduction performance for rGO/TNWs is seen to be even better than GO/TNWs (Figure 6b). On rGO/TNWs, total removal of Cr(VI) can be observed after 60 min of illumination. In contrast to the previous set of samples, regarding rGO/TNWs, the reduction is faster for thinner rGO samples. For example, a 10-s deposited sample showed total removal of Cr(VI) after 30 min. The thickness of the rGO is obviously dependent on the time of rGO deposition. Typically, based on FESEM cross-section images, the rGO deposited has thicknesses of 50–90 nm after >30-s of deposition. For shorter deposition times, the thickness can be estimated to be ~ 10–40 nm. Several samples were then used for reusability tests; nevertheless, it appears that the adherence of the rGO weakened after being used more than once. This could be due to the very acidic nature of the Cr(VI) solution and the variation of thickness of the rGO on the surface of the TNWs.

The PL spectra of TNW, GO/TNW, and rGO/TNW samples are shown in Figure 7. The clear PL peak centered at 570 nm may be related to defects that are recombination centers of the photogenerated electron-hole pairs. Some examples are oxygen vacancies, the K₂Ti₆O₁₃ phase, and interstitial defects within the TiO₂ lattice [40–42]. Recombination is obvious for the TNW sample but not for the GO/TNWs and very much reduced for the rGO/TNW sample. This is possibly the result of the rapid transfer of electrons from GO or rGO suppressing recombination [43,44]. With more free electrons available and higher mobility of electrons in rGO, a more rapid reduction process leads to a fast and complete removal of Cr(VI) within 30 min of exposure to visible light. Furthermore, the improved photoreduction performance of the rGO/TNWs compared to TNWs is attributed to the great enhancement of electron transport through the rGO in the rGO/TNW sample and its consequent charge separation.

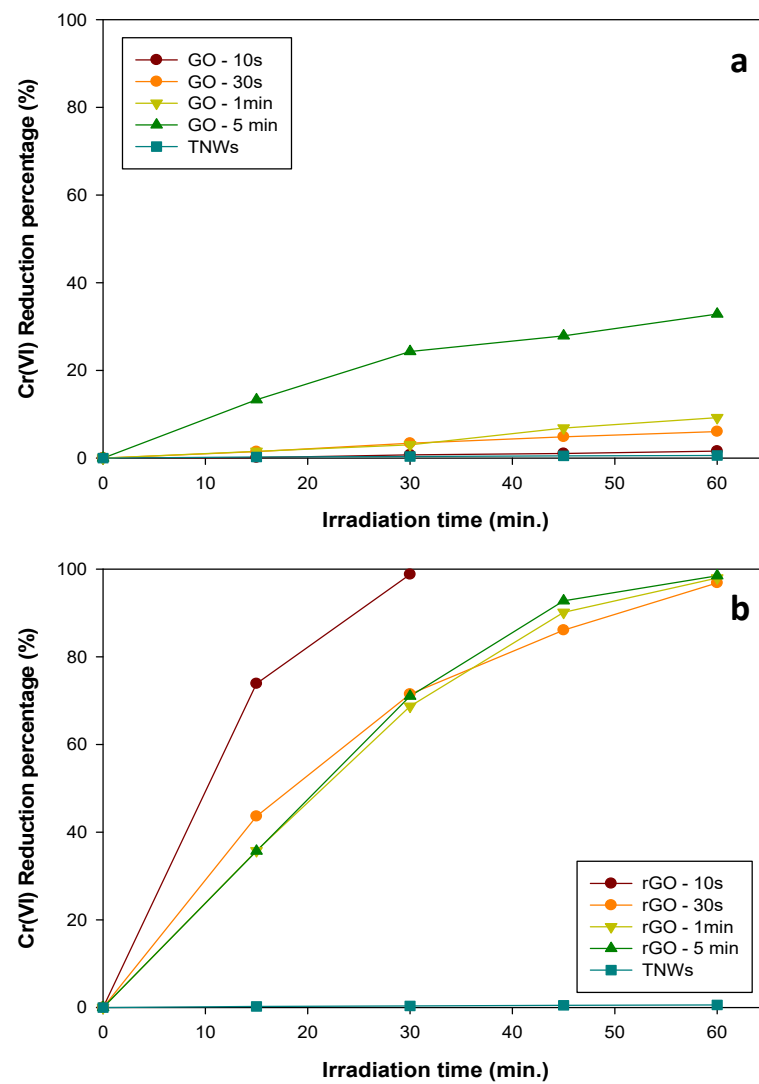


Figure 6. Photocatalytic reduction of Cr(VI) illuminated under visible light using different samples: (a) TNW and GO/TNW samples; and (b) TNW and rGO/TNW samples.

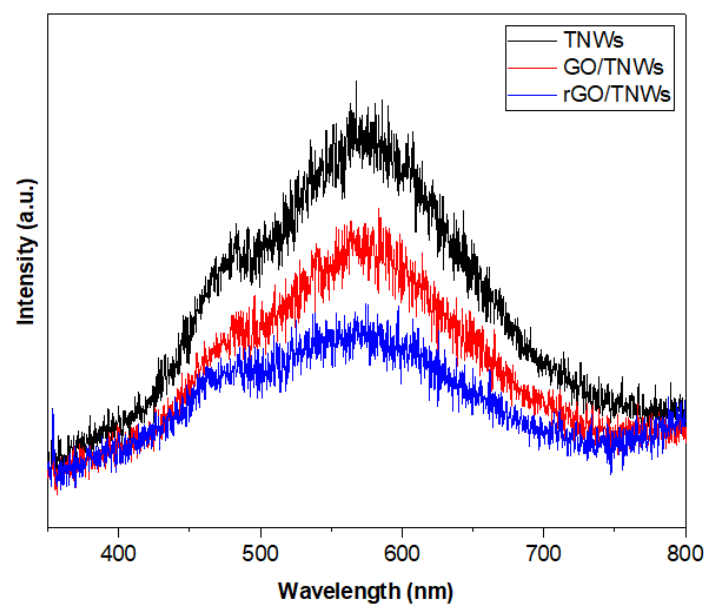


Figure 7. Photoluminescence spectra of TNW, GO/TNW, and rGO/TNW samples.

Table 1 compares this work with recent literature on the photoreduction of Cr(VI) [45–51]. It is evident that the photocatalytic reduction of rGO/TNWs formed in this work is comparable, if not superior, to the rGO/TiO₂ (nanoparticles) composite under visible light irradiation. Moreover, it is known that the addition of a scavenger can improve the efficiency of Cr(VI) photoreduction. There are several types of scavengers that can be used, and phenol is one of them. It can be seen from Table 1 that reduction in the presence of phenol (10 mM) is slower [46] than that of EDTA (this work), thus, concluding that EDTA is perhaps a better scavenger for this purpose.

Table 1. Comparison of obtained Cr(VI) reduction efficiency with recent studies under UV–Vis light irradiation (RGO = reduced graphene oxide; C = carbon).

Photocatalysts	Method	Sample Amount/Size	Scavenger	pH	Cr(VI) Conc. (ppm)	Source of Light	Removal Efficiency (%)	Time (min)	Ref.
TNTs-Air	Anodization	1 cm ²	–	2	10	Sunlight	10	180	[45]
C-Modified n-TiO ₂	Sol–gel	1 g/L	Phenol (10 mM)	5	5	Sunlight	100	120	[46]
TiO ₂ -5%rGO	Hydrothermal	–	–	2	10	Solar	98	180	[47]
TiO ₂ /rGO	Sol–gel	–	–	2.6	12	Mercury lamp	86.5	240	[38]
Mn-TiO ₂ /rGO	Hydrothermal	1 g/L	–	–	20	Sunlight	99.02	60	[48]
CoS ₂ /g-C ₃ N ₄ -rGO	Solvothermal	10 mg	–	2	20	350 W Xe lamp	99.8	150	[49]
TiO ₂ /rGO/CuO	Hydrothermal	50 mg	Citric acid (100 ppm)	–	100	500 W Au halide lamp	100	80	[50]
TiO ₂ /g-C ₃ N ₄ Microspheres/rGO	Hydrothermal	50 mg	–	3	100	300 W Xe lamp	97	240	[51]
TiO ₂ NW-RGO	Thermal Oxidation	4 cm ²	EDTA (1 mM)	1	10	Xenon lamp	100	30	This work

As mentioned previously, the use of a supported photocatalyst for Cr(VI) removal from contaminated water has several advantages, including better electron injection from rGO to TiO₂ and easy catalyst recovery after use. From Table 1, it is obvious from the literature that no other work has reported on the use of a supported photocatalyst such as that reported in this work. The majority of works reported on the used TiO₂ nanoparticles derived by sol-gel or a hydrothermal process. Anodization of titanium [45] produces a thin anodic film composed of TiO₂ nanotubes. Anodized titanium can therefore be considered catalyst support. However, Cr(VI) reduction on such anodized Ti (without rGO—or GO—deposition) is very slow, as shown in Table 1, indicating the importance of rGO for faster Cr(VI) reduction. The morphology of TNWs obtained in this study is also thought to provide a better anchor layer for the deposition of rGO nanosheets.

3. Materials and Methods

3.1. Synthesis of TiO₂ Nanowires

Titanium foils (0.10-mm-thick, 99.7% pure, 20 × 20 mm; Stream Chemical, USA) were first polished and then ultrasonically cleaned in acetone [(CH₃)₂CO, J. T. Baker-9254, Phillipsburg, NJ, USA], ethanol (C₂H₅OH, 95.7%, Samchem, Malaysia), and deionized water. The cleaned foils were placed in the hot zone of a horizontal tube furnace (Lenton 1200) for oxidation. The foils were oxidized using two heating profiles: first, at 400 °C for 10 min (heating rate = 5 °C/min), during which 1 M potassium hydroxide (KOH, Merck, Germany) mist was injected into the furnace, and second, at 750 °C (heating rate = 30 °C/min) for 120 min, during which water mist was injected into the furnace.

3.2. Synthesis of rGO Nanosheets

10 mg/L GO nanosheet solution (Tokyo Chemical Industry Ltd., Tokyo, Japan) was diluted with deionized water to obtain a 0.1 mg/L GO nanosheet solution. Then, 50 mL of the solution was ultrasonically dispersed for 15 min in an ultrasonic bath; 1 mg of ascorbic acid ($C_6H_8O_6$) was then added to the solution, and the solution was heated to 95 °C. Prior to the addition of ascorbic acid, the pH of the solution was adjusted to 10 using NaOH.

3.3. GO/rGO Deposition on TNWs Sample Using EPD

EPD was conducted in 0.1 mg/L GO or rGO solution as the electrolyte with TNWs connected to the positive terminal of a DC power supply (GWS Instek GPS 3303, Transfer Multisort Elektronik Ltd., Łódź, Poland) and a Pt rod connected to the negative terminal. EPD in both electrolytes was performed at various deposition times (10 s, 30 s, 1 min, and 5 min) at 20 V. After the EPD process, the sample was dried in an oven at 100 °C for 15 min.

3.4. Characterizations

The surface structural morphologies of the GO/TNWs and rGO/TNWs were observed using a field-emission-scanning electron microscope (FESEM; Zeiss Supra 35, Germany). Phase identification and crystal-structure analysis were based on data obtained from an X-ray diffractometer [XRD; Bruker Advanced X-ray Solution D8 with Cu-K α radiation ($\lambda = 0.154$ nm), United States] and a Raman spectrometer (Renishaw inVia Raman microscope, Gloucestershire, UK). Raman spectra were used to identify the presence of GO and rGO in the sample. Identification of chemical bonds in the sample was conducted by analyzing data from an X-ray photoelectron spectrometer [XPS; Kratos Axis Ultra with Al-K α radiation ($E_{\text{photons}} = 1486.7$ eV), Shimadzu Co., Ltd., Kyoto, Japan]. Photoluminescence studies were performed to identify impurities or defects that could be recombination centers of electron-hole pairs in the sample, using a monochromatic beam generated from a He-Cd laser (wavelength of 325 nm) and recorded using a monochromator (Nikon G250, Japan).

3.5. Cr (VI) Photoreduction Experiment

50 mL of the Cr(VI) (10 mg/L) solution was prepared by dissolving potassium dichromate salt ($K_2Cr_2O_7$) in distilled water. The pH value of the solution was adjusted to 2 by adding HCl solution. Then, 0.015 g of ethylene diamine tetra acetic acid was added to the solution and stirred for 5 min. GO/TNW or rGO/TNW samples were then immersed in the solution. The solution was then kept in the dark for 1 h prior to irradiation with visible light to achieve adsorption–desorption equilibrium. This was done using a solar simulator AM 1.5 (Xenon lamp, 1410 W/m² of intensity, LSPX150, Zolix Instruments Co. Ltd., Beijing, China). 3 mL aliquot samples were taken every 15 min during irradiation, and 1,5-diphenylcarbazide (DPC) was used to color the aliquot solution before subjecting it to measurement using a UV/Vis spectrometer (Varian Cary 50, Mulgrave, Australia).

4. Conclusions

GO or rGO deposition using the EPD method was carried out on TNWs. The TNWs were produced by thermal oxidation in the presence of KOH mist. rGO was obtained by the chemical reduction of commercially available GO using ascorbic acid. The fabricated TNW, GO/TNW, and rGO/TNW samples were used to reduce Cr(VI) in a photocatalysis experiment under simulated sunlight irradiation. It was found that a GO/TNW sample with 5 min of deposition was able to reduce 32.84% of the Cr(VI) ions after 1 h of irradiation, but rGO/TNWs with 10 s of deposition displayed a 100% reduction after 30 min of exposure to visible light. This could be due to the amount of transferred photogenerated electrons from GO or rGO to the TNWs.

Author Contributions: Conceptualization, S.T.R., N.A. and Z.L.; methodology, S.T.R. and Z.L.; validation, S.T.R., R.K., W.K.T., G.K., A.M. and Z.L.; formal analysis, S.T.R., N.A. and Z.L.; investigation, S.T.R., N.A. and Z.L.; resources, Z.L. and W.K.T.; data curation, S.T.R. and Z.L.; writing—original draft preparation, S.T.R. and Z.L.; writing—review and editing, R.K., W.K.T. and Z.L.; visualization, S.T.R., W.K.T. and Z.L.; supervision, Z.L.; project administration, W.K.T. and Z.L.; funding acquisition, W.K.T. and Z.L. All authors have read and agreed to the published version of the manuscript.

Funding: This research was funded by Fundamental Research Grant Scheme, Ministry of Higher Education Malaysia FRGS/1/2017/STG07/USM/02/4 (Z.L.) and the Japan Society for the Promotion of Science (JSPS) KAKENHI, grant numbers 21K18823, 21K18824 and 22K04737.

Acknowledgments: The authors would like to thank the Fundamental Research Grant Scheme, Ministry of Higher Education Malaysia FRGS/1/2017/STG07/USM/02/4 (Z.L.). A.M., G.K. and W.K.T. would like to acknowledge the JSPS KAKENHI Grant Numbers 21K18823, 21K18824 and 22K04737 for supporting this research. R.K. would like to acknowledge the Science and Engineering Research Board (SERB), Department of Science & Technology (DST) for financial support (SB/S2/RJN-159/2017). We thank Iain Mackie, from Edanz (<https://jp.edanz.com/>, accessed on 5 September 2022) for editing a draft of this manuscript.

Conflicts of Interest: The authors declare no conflict of interest.

References

1. Cheng, H.; Zhou, T.; Li, Q.; Lu, L.; Lin, C. Anthropogenic chromium emissions in China from 1990 to 2009. *PLoS ONE* **2014**, *9*, e87753. [CrossRef]
2. IARC (International Agency for Research on Cancer). List of Classifications, Volumes 1–132. 2022. Available online: http://monographs.iarc.fr/ENG/Classification/latest_classif.php (accessed on 31 August 2022).
3. Alias, N.; Hussain, Z.; Tan, W.K.; Kawamura, G.; Muto, H.; Matsuda, A.; Lockman, Z. Nanoporous anodic Nb₂O₅ with pore-in-pore structure formation and its application for the photoreduction of Cr(VI). *Chemosphere* **2021**, *283*, 131231. [CrossRef]
4. Goyer, G.; Golub, M.; Choudhury, H.; Hughes, M.; Kenyon, E.; Stifelman, M. *Issue Paper on The Human Health Effects of Metals*; U.S. Environmental Protection Agency: Washington, DC, USA, 2004.
5. Chen, X.; Mao, S.S. Titanium dioxide nanomaterials: Synthesis, properties, modifications, and applications. *Chem. Rev.* **2007**, *107*, 2891–2959. [CrossRef] [PubMed]
6. Rahmat, S.T.; Tan, W.K.; Kawamura, G.; Matsuda, A.; Lockman, Z. Synthesis of rutile TiO₂ nanowires by thermal oxidation of titanium in the presence of KOH and their ability to photoreduce Cr(VI) ions. *J. Alloys Compd.* **2020**, *812*, 152094. [CrossRef]
7. Du, J.; Gu, X.; Guo, H.; Liu, J.; Wu, Q.; Zou, J. Self-induced preparation of TiO₂ nanowires by chemical vapor deposition. *J. Cryst. Growth* **2015**, *427*, 54–59. [CrossRef]
8. Yun, G.; Song, G.Y.; Ahn, B.-E.; Lee, S.-K.; Heo, J.; Ahn, K.-S.; Kang, S.H. Beneficial surface passivation of hydrothermally grown TiO₂ nanowires for solar water oxidation. *Appl. Surf. Sci.* **2016**, *366*, 561–566. [CrossRef]
9. Attar, A.S.; Hassani, Z. Fabrication and growth mechanism of single-crystalline rutile TiO₂ nanowires by liquid-phase deposition process in a porous alumina template. *J. Mater. Sci. Technol.* **2015**, *31*, 828–833. [CrossRef]
10. Ge, M.; Li, Q.; Cao, C.; Huang, J.; Li, S.; Zhang, S.; Chen, Z.; Zhang, K.; Al-Deyab, S.S.; Lai, Y. One-dimensional TiO₂ nanotube photocatalysts for solar water splitting. *Adv. Sci.* **2017**, *4*, 1600152. [CrossRef]
11. Hejazi, S.; Pour-Ali, S.; Killian, M.S.; Mohajernia, S. One-dimensional suboxide TiO₂ nanotubes for electrocatalytic applications. *Electrochem. Commun.* **2022**, *136*, 107246. [CrossRef]
12. Mangham, A.N.; Govind, N.; Bowden, M.E.; Shutthanandan, V.; Joly, A.G.; Henderson, M.A.; Chambers, S.A. Photochemical properties, composition, and structure in molecular beam epitaxy grown Fe “doped” and (Fe,N) codoped rutile TiO₂(110). *J. Phys. Chem. C* **2011**, *115*, 15416–15424. [CrossRef]
13. Xu, M.; Shao, S.; Gao, B.; Lv, J.; Li, Q.; Wang, Y.; Wang, H.; Zhang, L.; Ma, Y. Anatase (101)-like structural model revealed for metastable rutile TiO₂(011) surface. *ACS Appl. Mater. Interfaces* **2017**, *9*, 7891–7896. [CrossRef]
14. Asahi, R.; Morikawa, T.; Irie, H.; Ohwaki, T. Nitrogen-doped titanium dioxide as visible-light-sensitive photocatalyst: Designs, developments, and prospects. *Chem. Rev.* **2014**, *114*, 9824–9852. [CrossRef]
15. Pan, J.; Li, C.; Zhao, Y.; Liu, R.; Gong, Y.; Niu, L.; Liu, X.; Chi, B. Electronic properties of TiO₂ doped with Sc, Y, La, Zr, Hf, V, Nb and Ta. *Chem. Phys. Lett.* **2015**, *628*, 43–48. [CrossRef]
16. Xiao, L.; Li, Y.; Chen, F.; Xu, P.; Li, M. Facile synthesis of mesoporous titanium dioxide doped by Ag-coated graphene with enhanced visible-light photocatalytic performance for methylene blue degradation. *RSC Adv.* **2017**, *7*, 25314–25324. [CrossRef]
17. Khairy, M.; Zakaria, W. Effect of metal-doping of TiO₂ nanoparticles on their photocatalytic activities toward removal of organic dyes. *Egypt. J. Pet.* **2014**, *23*, 419–426. [CrossRef]
18. Kumar, R.; Sahoo, S.; Joanni, E.; Singh, R.K.; Tan, W.K.; Kar, K.K.; Matsuda, A. Recent progress on carbon-based composite materials for microwave electromagnetic interference shielding. *Carbon* **2021**, *177*, 304–331. [CrossRef]

19. Kumar, R.; Sahoo, S.; Tan, W.K.; Kawamura, G.; Matsuda, A.; Kar, K.K. Microwave-assisted thin reduced graphene oxide-cobalt oxide nanoparticles as hybrids for electrode materials in supercapacitor. *J. Energy Storage* **2021**, *40*, 102724. [[CrossRef](#)]
20. Youssry, S.M.; El-Hallag, I.S.; Kumar, R.; Kawamura, G.; Matsuda, A.; El-Nahass, M.N. Synthesis of mesoporous Co(OH)₂ nanostructure film via electrochemical deposition using lyotropic liquid crystal template as improved electrode materials for supercapacitors application. *J. Electroanal. Chem.* **2020**, *857*, 113728. [[CrossRef](#)]
21. Kumar, R.; Sahoo, S.; Joanni, E.; Singh, R.K.; Yadav, R.M.; Verma, R.K.; Singh, D.P.; Tan, W.K.; Pérez del Pino, A.; Moshkalev, S.A.; et al. A review on synthesis of graphene, h-BN and MoS₂ for energy storage applications: Recent progress and perspectives. *Nano Res.* **2019**, *12*, 2655–2694. [[CrossRef](#)]
22. Tan, W.K.; Asami, K.; Maegawa, K.; Kumar, R.; Kawamura, G.; Muto, H.; Matsuda, A. Fe₃O₄-embedded rGO composites as anode for rechargeable FeOx-air batteries. *Mater. Today Commun.* **2020**, *25*, 101540. [[CrossRef](#)]
23. Kumar, R.; Sahoo, S.; Joanni, E.; Singh, R.K.; Tan, W.K.; Kar, K.K.; Matsuda, A. Recent progress in the synthesis of graphene and derived materials for next generation electrodes of high performance lithium ion batteries. *Prog. Energy Combust. Sci.* **2019**, *75*, 100786. [[CrossRef](#)]
24. Zhang, L.W.; Fu, H.B.; Zhu, Y.F. Efficient TiO₂ photocatalysts from surface hybridization of TiO₂ particles with graphite-like carbon. *Adv. Funct. Mater.* **2008**, *18*, 2180–2189. [[CrossRef](#)]
25. Neto, A.C.; Guinea, F.; Peres, N.M.; Novoselov, K.S.; Geim, A.K. The electronic properties of graphene. *Rev. Mod. Phys.* **2009**, *81*, 109. [[CrossRef](#)]
26. Tayebi, M.; Kolaei, M.; Tayyebi, A.; Masoumi, Z.; Belbasi, Z.; Lee, B.K. Reduced graphene oxide (RGO) on TiO₂ for an improved photoelectrochemical (PEC) and photocatalytic activity. *Sol. Energy* **2019**, *190*, 185–194. [[CrossRef](#)]
27. An, S.J.; Zhu, Y.; Lee, S.H.; Stoller, M.D.; Emilsson, T.; Park, S.; Velamakanni, A.; An, J.; Ruoff, R.S. Thin film fabrication and simultaneous anodic reduction of deposited graphene oxide platelets by electrophoretic deposition. *J. Phys. Chem. Lett.* **2010**, *1*, 1259–1263. [[CrossRef](#)]
28. Liu, X.; Pan, L.; Lv, T.; Zhu, G.; Lu, T.; Sun, Z.; Sun, C. Microwave-assisted synthesis of TiO₂-reduced graphene oxide composites for the photocatalytic reduction of Cr(VI). *RSC Adv.* **2011**, *1*, 1245–1249. [[CrossRef](#)]
29. Ilie, A.G.; Scarisoareanu, M.; Morjan, I.; Dutu, E.; Badiceanu, M.; Mihailescu, I. Principal component analysis of Raman spectra for TiO₂ nanoparticle characterization. *Appl. Surf. Sci.* **2017**, *417*, 93–103. [[CrossRef](#)]
30. He, A.; Chen, G.; Chen, J.; Peng, J.; Srinivasakannan, C.; Ruan, R. A novel method of synthesis and investigation on transformation of synthetic rutile powders from Panzhihua sulphate titanium slag using microwave heating. *Powder Technol.* **2018**, *323*, 115–119. [[CrossRef](#)]
31. Meng, X.; Wang, D.; Liu, J.; Lin, B.; Fu, Z. Effects of titania different phases on the microstructure and properties of K₂Ti₆O₁₃ nanowires. *Solid State Commun.* **2006**, *137*, 146–149. [[CrossRef](#)]
32. Wang, M.; Duong, L.D.; Oh, J.-S.; Mai, N.T.; Kim, S.; Hong, S.; Hwang, T.; Lee, Y.; Nam, J.-D. Large-area, conductive and flexible reduced graphene oxide (RGO) membrane fabricated by electrophoretic deposition (EPD). *ACS Appl. Mater. Interfaces* **2014**, *6*, 1747–1753. [[CrossRef](#)]
33. Kumar, R.; Youssry, S.M.; Abdel-Galeil, M.M.; Matsuda, A. One-pot synthesis of reduced graphene oxide nanosheets anchored ZnO nanoparticles via microwave approach for electrochemical performance as supercapacitor electrode. *J. Mater. Sci. Mater. Electron.* **2020**, *31*, 15456–15465. [[CrossRef](#)]
34. Kumar, R.; da Silva, E.T.S.G.; Singh, R.K.; Savu, R.; Alaferdov, A.V.; Fonseca, L.C.; Carossi, L.C.; Singh, A.; Khandka, S.; Kar, K.K.; et al. Microwave-assisted synthesis of palladium nanoparticles intercalated nitrogen doped reduced graphene oxide and their electrocatalytic activity for direct-ethanol fuel cells. *J. Colloid Interface Sci.* **2018**, *515*, 160–171. [[CrossRef](#)]
35. Kumar, R.; Singh, R.K.; Vaz, A.R.; Savu, R.; Moshkalev, S.A. Self-assembled and one-step synthesis of interconnected 3D network of Fe₃O₄/reduced graphene oxide nanosheets hybrid for high-performance supercapacitor electrode. *ACS Appl. Mater. Interfaces* **2017**, *9*, 8880–8890. [[CrossRef](#)]
36. Stankovich, S.; Dikin, D.A.; Piner, R.D.; Kohlhaas, K.A.; Kleinhammes, A.; Jia, Y.; Wu, Y.; Nguyen, S.T.; Ruoff, R.S. Synthesis of graphene-based nanosheets via chemical reduction of exfoliated graphite oxide. *Carbon* **2007**, *45*, 1558–1565. [[CrossRef](#)]
37. Žerjav, G.; Arshad, M.S.; Djinović, P.; Junkar, I.; Kovač, J.; Zavašnik, J.; Pintar, A. Improved electron–hole separation and migration in anatase TiO₂ nanorod/reduced graphene oxide composites and their influence on photocatalytic performance. *Nanoscale* **2017**, *9*, 4578–4592. [[CrossRef](#)]
38. Zhao, Y.; Zhao, D.; Chen, C.; Wang, X. Enhanced photo-reduction and removal of Cr(VI) on reduced graphene oxide decorated with TiO₂ nanoparticles. *J. Colloid Interface Sci.* **2013**, *405*, 211–217. [[CrossRef](#)] [[PubMed](#)]
39. Taib, M.A.A.; Razak, K.A.; Jaafar, M.; Lockman, Z. Initial growth study of TiO₂ nanotube arrays anodised in KOH/fluoride/ethylene glycol electrolyte. *Mater. Des.* **2017**, *128*, 195–205. [[CrossRef](#)]
40. Wu, J.-M.; Shih, H.C.; Wu, W.-T. Formation and photoluminescence of single-crystalline rutile TiO₂ nanowires synthesized by thermal evaporation. *Nanotechnology* **2005**, *17*, 105. [[CrossRef](#)]
41. Shi, J.; Chen, J.; Feng, Z.; Chen, T.; Lian, Y.; Wang, X.; Li, C. Photoluminescence characteristics of TiO₂ and their relationship to the photoassisted reaction of water/methanol mixture. *J. Phys. Chem. C* **2007**, *111*, 693–699. [[CrossRef](#)]
42. Schneider, J.; Matsuoka, M.; Takeuchi, M.; Zhang, J.; Horiuchi, Y.; Anpo, M.; Bahnemann, D.W. Understanding TiO₂ photocatalysis: Mechanisms and materials. *Chem. Rev.* **2014**, *114*, 9919–9986. [[CrossRef](#)] [[PubMed](#)]

43. Yang, N.; Zhai, J.; Wang, D.; Chen, Y.; Jiang, L. Two-dimensional graphene bridges enhanced photoinduced charge transport in dye-sensitized solar cells. *ACS Nano* **2010**, *4*, 887–894. [[CrossRef](#)]
44. Fernández-Merino, M.J.; Guardia, L.; Paredes, J.; Villar-Rodil, S.; Solís-Fernández, P.; Martínez-Alonso, A.; Tascon, J. Vitamin C is an ideal substitute for hydrazine in the reduction of graphene oxide suspensions. *J. Phys. Chem. C* **2010**, *114*, 6426–6432. [[CrossRef](#)]
45. Bashir, N.; Tan, W.K.; Kawamura, G.; Matsuda, A.; Lockman, Z. Comparison of ZrO₂, TiO₂, and α-Fe₂O₃ nanotube arrays on Cr(VI) photoreduction fabricated by anodization of Zr, Ti, and Fe foils. *Mater. Res. Express* **2020**, *7*, 055013. [[CrossRef](#)]
46. Shaban, Y.A. Effective photocatalytic reduction of Cr(VI) by carbon modified (CM)-n-TiO₂ nanoparticles under solar irradiation. *World J. Nano Sci. Eng.* **2013**, *3*, 154–160. [[CrossRef](#)]
47. Liu, L.; Luo, C.; Xiong, J.; Yang, Z.; Zhang, Y.; Cai, Y.; Gu, H. Reduced graphene oxide (rGO) decorated TiO₂ microspheres for visible-light photocatalytic reduction of Cr(VI). *J. Alloys Compd.* **2017**, *690*, 771–776. [[CrossRef](#)]
48. Chen, Z.; Li, Y.; Guo, M.; Xu, F.; Wang, P.; Du, Y.; Na, P. One-pot synthesis of Mn-doped TiO₂ grown on graphene and the mechanism for removal of Cr(VI) and Cr(III). *J. Hazard Mater.* **2016**, *310*, 188–198. [[CrossRef](#)]
49. Wang, Y.; Bao, S.; Liu, Y.; Yang, W.; Yu, Y.; Feng, M.; Li, K. Efficient photocatalytic reduction of Cr(VI) in aqueous solution over CoS₂/g-C₃N₄-rGO nanocomposites under visible light. *Appl. Surf. Sci.* **2020**, *510*, 145495. [[CrossRef](#)]
50. Wang, N.; Zhang, F.; Mei, Q.; Wu, R.; Wang, W. Photocatalytic TiO₂/rGO/CuO Composite for Wastewater Treatment of Cr(VI) Under Visible Light. *Water Air Soil Pollut.* **2020**, *231*, 223. [[CrossRef](#)]
51. Li, G.; Wu, Y.; Zhang, M.; Chu, B.; Huang, W.; Fan, M.; Dong, L.; Li, B. Enhanced Removal of Toxic Cr(VI) in Wastewater by Synthetic TiO₂/g-C₃N₄ Microspheres/rGO Photocatalyst under Irradiation of Visible Light. *Ind. Eng. Chem. Res.* **2019**, *58*, 8979–8989. [[CrossRef](#)]